Experimental and numerical study of bending-induced buckling of stiffened composite plate assemblies

Telford, R.; Peeters, D. M.J.; Rouhi, M.; Weaver, P. M.

DOI
10.1016/j.compositesb.2022.109642

Publication date
2022

Document Version
Final published version

Published in
Composites Part B: Engineering

Citation (APA)
Telford, R., Peeters, D. M. J., Rouhi, M., & Weaver, P. M. (2022). Experimental and numerical study of bending-induced buckling of stiffened composite plate assemblies. *Composites Part B: Engineering*, *233*, Article 109642. https://doi.org/10.1016/j.compositesb.2022.109642

Composites Part B 233 (2022) 109642

Contents lists available at ScienceDirect

Composites Part B

journal homepage: www.elsevier.com/locate/compositesb

Experimental and numerical study of bending-induced buckling of stiffened composite plate assemblies

R. Telford [a], D.M.J. Peeters [a,b], M. Rouhi [a,*], P.M. Weaver [a]

[a] Bernal Institute, University of Limerick, Co., Limerick, V94 T9PX, Ireland
[b] Faculty of Aerospace Engineering, Delft University of Technology, Kluyverweg 1, Delft, 2629 HS, the Netherlands

ARTICLE INFO

Keywords:
Buckling
Test method
Automated fibre placement
Thermoplastic composite

ABSTRACT

Despite their importance in benchmarking numerical simulations, buckling tests still feature compromises between component-level and high-fidelity large-scale tests. For example, compression-induced buckling tests cannot capture the through-thickness or span-wise stress gradients in wing skins. Consequently, the results obtained often require careful interpretation and conservative considerations before applying to a structure. Alternatively, a system-level large-scale test can be used, yet at considerably increased time and expense. There has been little progression towards capturing system-level behaviour in a simplified test.

Herein, for buckling behaviour assessment, a three-point bending test is used, which is quick, simple to implement, and cost-effective compared to existing conventional methods. The proposed method relies on subjecting a panel with auxiliary stiffeners to bending to introduce compression-induced buckling in the skin. The three-point bend test is used, because it provides readily controllable loading and boundary conditions. The location of the neutral plane can be tailored via design of the stiffeners, thus allowing for control of the through-thickness stress gradient induced in the skin. This method is applicable to buckling of stiffened structures subject to bending (e.g., aircraft wingboxes). Numerical models are used to explore the limits of the proposed method and comparing it against traditional coupon and full-scale structural level tests. The test method is experimentally demonstrated for capturing the buckling behaviour of a thermoplastic composite panel made via automated fibre placement. The proposed approach is shown to reliably capture the buckling behaviour of a large-scale test using a simpler and more time and cost-efficient setup than conventional methods.

1. Introduction

Buckling is defined as a structural instability (typically, a bifurcation) in which a thin-walled structural member changes shape by deforming in the out-of-plane direction at a load below its material strength limits. Structural designers rely on a combination of numerical predictions and structural tests to verify that there is sufficient margin to the buckling load. In weight and cost-sensitive structures (e.g., aircraft wings or wind-turbine blades), an accurate buckling load prediction method is an important element in development of optimised, light weight components.

Design tools, such as Finite Element Modelling (FEM) must be followed by representative test data for validation purposes. Traditionally, experimental data are extracted from using either compression or bending-induced buckling tests [1,2] or large-scale structural tests [3,4], each of which has its own shortcomings. Pure compression tests rely on bespoke frames to carefully apply boundary conditions (such as knife edge or clamped conditions) according to the structural configuration. However, pure compression tests do not fully represent the skin loading conditions in many non-uniform bending – feature an in-plane stress gradient along the skin due to the non-uniform bending moment. On the other hand, large-scale system-level tests, which correctly capture the stress distribution, are complex and expensive to implement. The proposed test method in this paper aims to bridge the gap between the two test methods.

Small-scale buckling tests often involves subjecting a coupon- or element-level specimen (with necessary structural detail) to pure compression, with the boundary conditions of all edges carefully controlled to replicate different structural configurations (generally between simply-supported and clamped) [1,5,6]. Pure compression is achieved by applying a displacement at one edge and fixing the other edge so that no variation in displacements is possible along those edges.

* Corresponding author.
E-mail address: mohammad.rouhi@ul.ie (M. Rouhi).

https://doi.org/10.1016/j.compositesb.2022.109642
Received 23 June 2021; Received in revised form 22 November 2021; Accepted 9 January 2022
Available online 13 January 2022

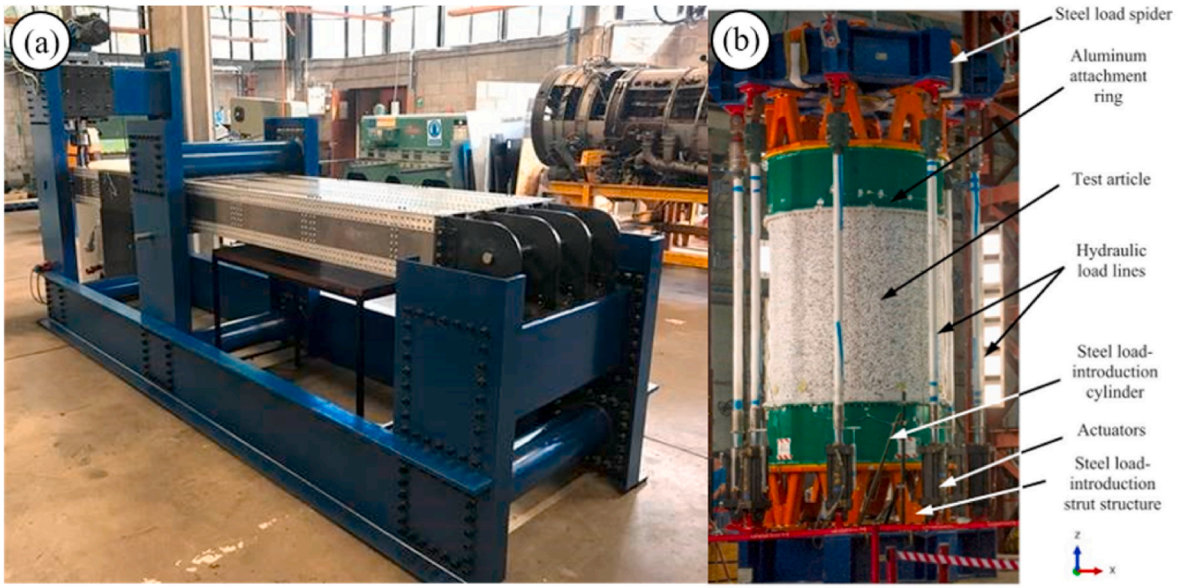

Fig. 1. Structural level buckling test (a) for a wingbox section, described in Ref. [4] and (b) a 8.33 ft tall, 8 ft diameter composite sandwich cylinder tested in axial compression [15].

The boundary conditions must be chosen to best match the behaviour of the structure in question, by means of controlling the degrees-of-freedom of each edge. Experimentally, this scenario is achieved by fitting a panel into a bespoke frame which has a combination of simply supported and clamped edges. While simple to model simply supported conditions in finite element software [7], this test has some drawbacks. Firstly, the test frame must be custom-designed and manufactured for each test configuration, including sufficient stiffness to replicate the loading conditions, while not unduly influencing the test. Achieving the appropriate level and type of boundary support can require intricate mechanisms, such as spring supports [5], which is a time-consuming and often unreliable exercise. Secondly, the test is highly sensitive to misalignments, imperfections, or 'off-ideal' conditions, which are difficult to control and lead to scattered test data and variations from predictions [6,8]. Consequently, further analysis and interpretation is required. Finally, the test is limited to pure compression. Structural interactions which give rise to stress gradients (in-plane or through-thickness) are not represented in such tests.

Plates and panels are usually stiffened in structural applications to avoid global buckling phenomena. For stiffened panel structures, the idealisation of pure compression has also been used analytically and experimentally [9–11]. This approach assumes that the stiffeners and the skin are subject to a single, constant displacement. Experimentally, such a scenario is achieved by encasing the loaded edges of the panel (including the stiffener) in a potting compound [12,13], resulting in a sufficiently stiff support such that effectively a clamped boundary condition arises. In case of non-stiffened components, reinforcement of the edges at the boundary or load introduction edges are also required in addition to potting to eliminate what would otherwise be unrealistic and dominant boundary effects [14]. The alignment of the specimen is important in this circumstance, to ensure that the specimen remains vertical during loading and that pure compression is achieved. In some cases, Computer Numerically Controlled (CNC) machining is required for the blocks to provide sufficient alignment accuracy [10]. While some interaction from the stiffener is considered in this case, it is not representative of an actual stiffened structure. Such structures are often used in bending, due to their large second moment of area. In these cases, stress gradients occur in the area between stiffeners, which can alter the buckling behaviour and are not considered in pure compression tests [14]. The in-plane (normal) stress gradient that results from the variation in bending moment is not considered in such tests, and neither are the through-thickness stress gradients in the skin material due to the distance to the neutral axis. Therefore, this type of test may not capture the physics of an actual structure sufficiently well, and the structural relevance of these tests may be limited.

One method of overcoming some of the shortcomings of traditional tests is to use a large scale, 'component' level structural test. Such a test uses a complete section of a structure (e.g., a wingbox or large composite sandwich cylinder), loaded in a representative manner [2,15]. The stresses induced in the area of interest are representative of the actual structure in this case. However, manufacturing a scale or full-size section of a structure is a significant undertaking, requiring considerable time and expense. Likewise, introducing the loads in a representative manner requires careful thought and the development of a bespoke testing solution. The wingbox structural level buckling test shown in Fig. 1(a), for example, required a large test frame, with 0.6 m and 2.5 m long aluminium wing box sections which were constructed with the sole purpose of introducing diffused loads and representative boundary conditions into the test section. Similarly, the cylindrical section tested shown in Fig. 1(b) requires load diffusion structures (green sections above and below the cylinder) to adequately diffuse the loads into the cylinder. Currently, no compromise exists between high-fidelity large-scale tests, which are complex, time consuming and expensive, and small-scale tests, which are cheaper and simpler but use idealised loading conditions. There is scope, therefore, for a sub-scale test to bridge the gap between these two approaches.

Over the years much research has been performed on buckling tests and bridge the gap between full-scale and coupon tests. For example, the testing of curved composite stiffened panels [16,17], and research into making a single-stiffener specimen representative of large panels with multiple stiffeners [18,19]. These tests remain very sensitive to the applied boundary conditions. Another example of simplified buckling tests is the scaling of sandwich composite cylindrical structures [3] and their testing [15]. The one thing all these works have in common is that pure compression load is used, which is not always representative of the true loading condition (such as in a wingbox).

The aim of this work is to propose another test to bridge the gap between small-scale (coupon/element level) and large-scale (component/system level) tests with a test that can capture the appropriate loading and boundary conditions of stiffened structures, such as the wingbox, while being less expensive to perform than the full-scale test. This objective is achieved by means of a new simple, cost-effective and

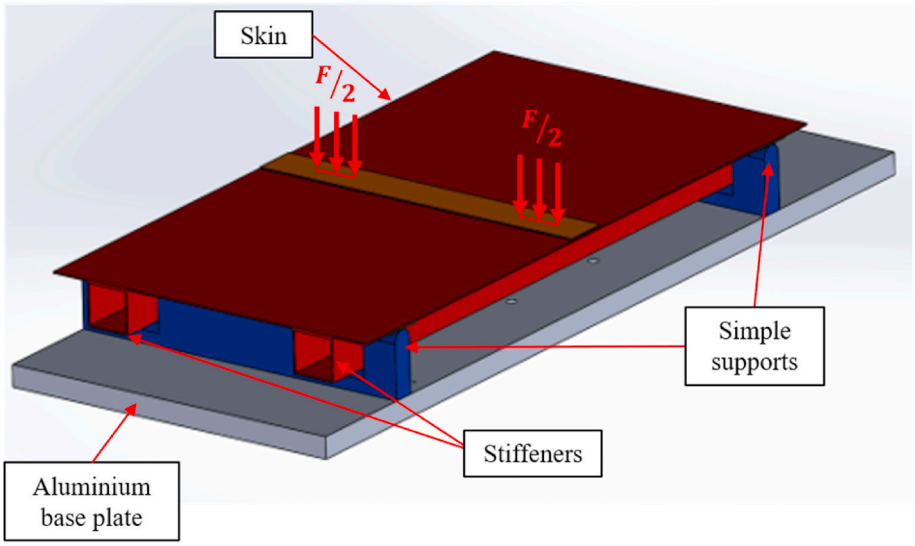

Fig. 2. Stiffened panel three-point bending test configuration. The stiffened panel (red) rests on the simple-supports (blue), which are mounted on a rigid base-plate (grey). The force F is applied directly above the two stringers. (For interpretation of the references to colour in this figure legend, the reader is referred to the Web version of this article.)

representable test design for buckling. The proposed test subjects a stiffened skin section to bending via the well-known three-point bending test to achieve a compressive load in the panel. Compared to regular 'pure-compression' tests, this test involves simple boundary conditions and alignment, reduced specimen preparation, and provides more representative loading conditions, i.e. compression in the skin section which has a tailored gradient through its gauge to fit the conditions of, for example, a wingbox skin. The boundary conditions are also more representative of the conditions in a full-scale test than those achieved in a coupon test. The complete test setup is described in Section 2. A comparison of this test, a large-scale structural level test, and the traditional pure compression test is given in Section 3 by means of a parametric study using Finite Element (FE) models. The proposed method is then demonstrated experimentally in Section 4. Finally, the proposed test is discussed in terms of its applicability, tailorability, and special considerations in Section 5.

2. Flexural test buckling method

Consider a stiffened panel structure, comprising a skin section with a number of stiffeners. If this section is loaded in bending (as, for example, in an aircraft wing), both upper and lower skin sections can be subjected to compressive loads, by considering both up and down bending of the overall wing. Our new test method considers such a skin section as being bonded to two parallel stiffeners. The panel is subjected to a three-point bending load (see Fig. 2), according to the well-known three-point bend test. However, in the current set-up the panel is not tested in bending but rather in compression, which is induced by bending in this case. The loads are applied directly to the skin above the stiffeners only, and not across the skin section between stiffeners. Consequently, compressive forces are introduced into the skin as a result of interfacial shear stresses developing between the stiffeners and skin – representing a scenario for a stiffened skin section.

The static scheme, shown in Fig. 2, relies on two simply supported boundary conditions (accomplished by using rounded edges for the support), and a rounded nose used for load introduction which allows rotations and translations.

Table 1
Material properties of CFRP and aluminium used in FE simulations.

Material	E_{11} (GPa)	E_{22} (GPa)	G_{12} (GPa)	ν_{12}
Tenax®-E TPUD PEEK IMS65	135	7.54	5	0.3
Al-6063T6	68.9 [20]			0.33 [20]

3. Comparison of the proposed test method against compression tests in representing structural level test

3.1. Parametric study

The usefulness of this test method rests on its ability to capture structural level behaviour in a small, simple test set-up. A comparison of buckling behaviour is performed using a parametric study, between the buckling response of traditional pure compression test [1], the proposed stiffened panel method, and the structural level test (represented by a wingbox section) [4]. As a result, this study demonstrates how the proposed component-level test method is more efficient and accurate in capturing the buckling behaviour of a panel as a subcomponent of a large structure, rather than performing a full-scale structural test.

Previous in-house research included the testing of a full-scale composite wingbox section, subjected to a shear force of 23.8 kN, which resulted in a bending moment of 14.3 kNm, [4]. Experimental and FE simulation results from this test are available for comparison against the proposed test method. In all cases, the skin section of interest (where buckling occurs) comprised eight layers of 0.18 mm thick unidirectional Carbon Fibre Reinforced Plastic (CFRP) thermoplastic prepreg with properties listed in Table 1. The material data of the Tenax material in Table 1 were obtained using in-house tests while designing the wingbox [4]. A lay-up sequence of $[90/0/\pm\theta]_s$ was used, with θ varying from 0° to 90° in 15° increments. Buckling load variation with θ can be examined for each structure, providing insight into the mechanisms at play, and allowing for a comparison of the small-scale test (pure compression) and the intermediate test (stiffened panel) against the structural level test.

The wingbox section examined is shown in Fig. 3; a one-piece, unitised composite structure with 3 closed Ω-shaped stiffeners on both upper and lower skins. The FE model used for buckling load analysis is described in prior work [4], and was successfully validated against experiments. For this study, the lay-ups used in the FE model of the

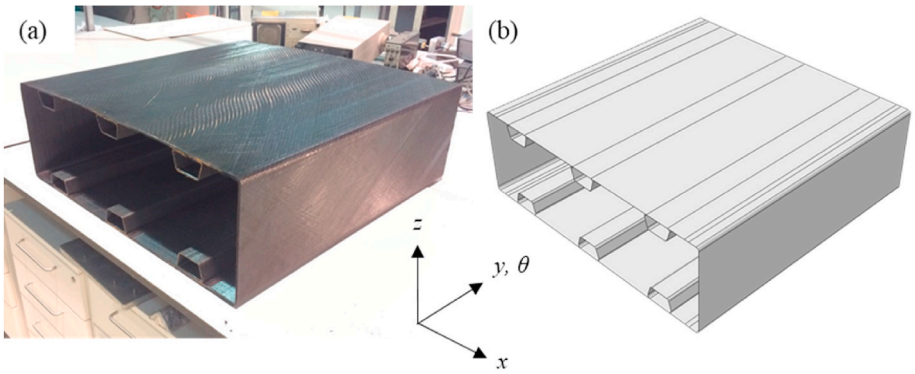

Fig. 3. (a) Wingbox demonstrator used for parametric study; and (b) wingbox geometric model configuration used in the FE parametric study.

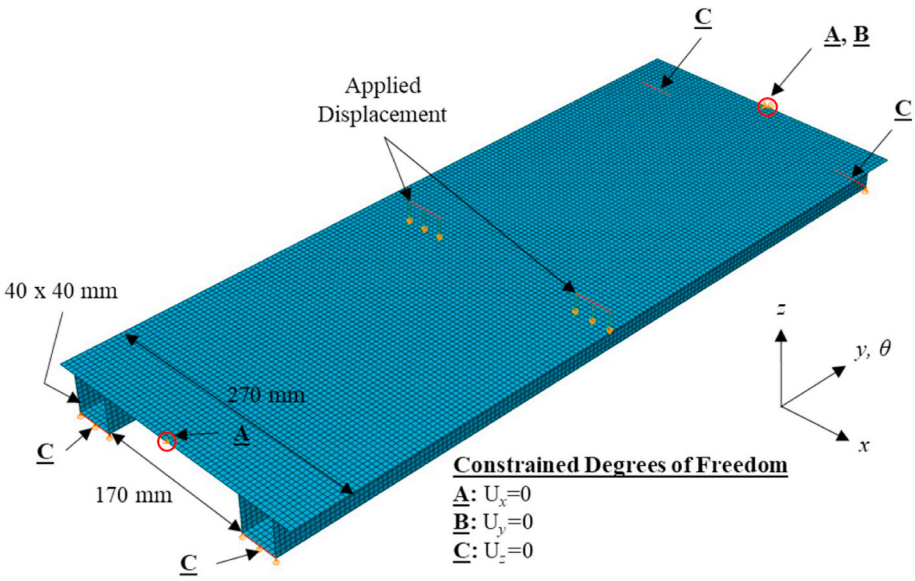

Fig. 4. Boundary conditions and mesh of flexural test case.

wingbox were modified from those used previously [4] to match those of the stiffened panel tested.

The stiffened panel was modelled as a corresponding skin section of the wingbox, with two stiffeners 170 mm apart. Square box section aluminium stiffeners of 40 mm wide were chosen in place of the Ω-shaped stiffeners to facilitate experiments (which are described in Section 4). It is worth noting that the stiffeners in this test are used only to offset the load and provide similar boundary conditions to the plate in between them, as in the wingbox test. Therefore, their exact shape is not important. The boundary conditions and loads are applied as per Fig. 4, which corresponds to the three-point bend test set-up with loads applied directly to the stiffeners. Four different lengths L were considered – 450 mm, 750 mm, 1500 mm, and 3400 mm – whilst the total width was 270 mm.

Finally, the pure compression tests were simulated as a section of skin material only, with no stiffeners (as per [1]). The gauge area of the test panels corresponds to the skin area between stiffeners in the wingbox (375 mm × 170 mm). Both simply supported and clamped boundary conditions were simulated. The mesh and boundary conditions used are shown in Fig. 5.

The simulations were carried out using ABAQUS, commercial FE solver to perform a linear buckling analysis. All models used four-noded reduced integration (S4R) shell elements due to the small thickness-to-length/width ratio. The material was idealised as linear elastic using the 'composite' shell in ABAQUS, meaning the lamina was defined as base material and the different fibre angles were defined in the ABAQUS interface. Internally, ABAQUS uses classical laminate theory to calculate the laminate stiffnesses based on the given lay-up. The element size was kept constant across models using a 5 mm length of the side. The buckling load was found using a linear perturbation step in ABAQUS. The mesh density decided upon after a mesh refinement study resulted in insignificant change in the buckling behaviour predicted, and particular attention given to ensure that the geometrical offsets were correctly applied. Finally, a perfect bond was assumed for the stiffener/skin interface. This assumption is appropriate as the interface is located far from the neutral axis of the plate assembly subject to bending, and therefore, the shear stresses generated at the stringer-to-panel interface remain small, resulting in no debonding occurring during the test. Indeed, no debonding was observed during testing, as is discussed further in section 4.3.2.

3.2. Results of parametric study

The results of the FE parametric study are shown in Figs. 6 and 7, with the buckling load as a function of fibre orientation θ being presented (note that θ is orientated parallel to the stiffeners, see Figs. 3–4). Each configuration is normalised to the maximum of that configuration. It is shown that the buckling load of the wingbox structure (as in Fig. 3, and represented by the black lines in Figs. 6 and 7) increases as θ increases from a minimum of $\theta = 0°$, with a maximum buckling load at $\theta =$

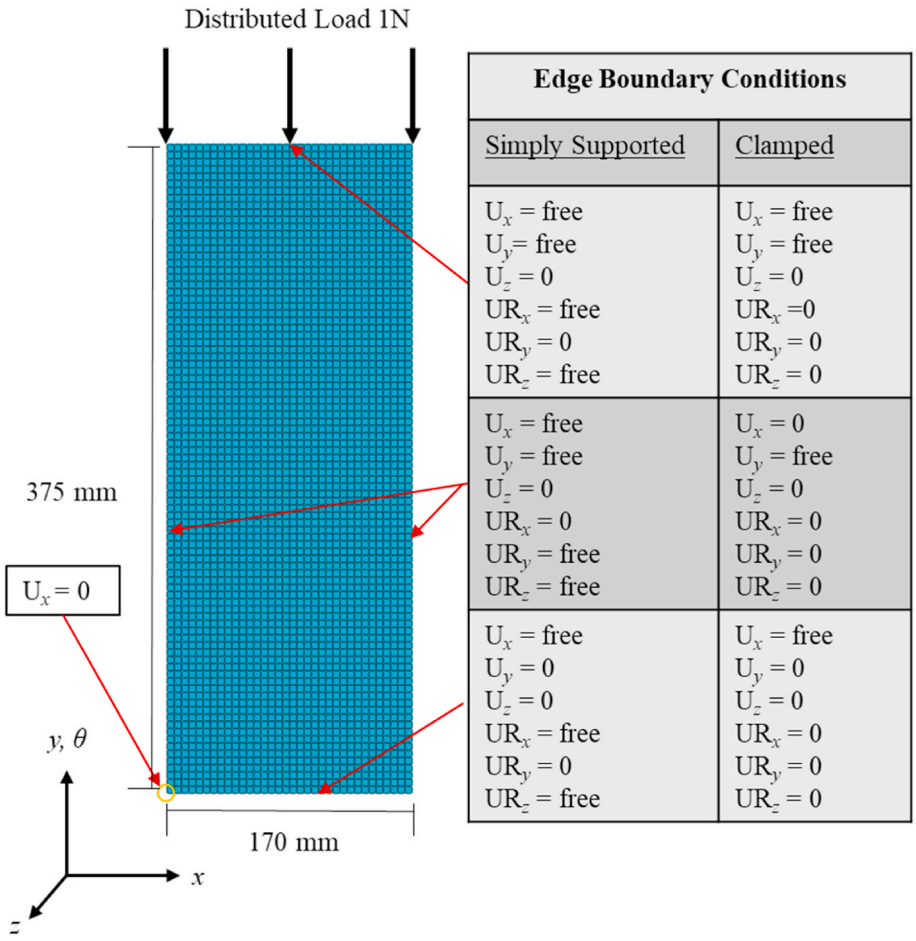

Edge Boundary Conditions	
Simply Supported	Clamped
U_x = free U_y = free U_z = 0 UR_x = free UR_y = 0 UR_z = free	U_x = free U_y = free U_z = 0 UR_x =0 UR_y = 0 UR_z = 0
U_x = free U_y = free U_z = 0 UR_x = 0 UR_y = free UR_z = free	U_x = 0 U_y = free U_z = 0 UR_x = 0 UR_y = 0 UR_z = 0
U_x = free U_y = 0 U_z = 0 UR_x = free UR_y = 0 UR_z = free	U_x = free U_y = 0 U_z = 0 UR_x = 0 UR_y = 0 UR_z = 0

Fig. 5. FE model boundary conditions used for simply supported and clamped pure compression simulations.

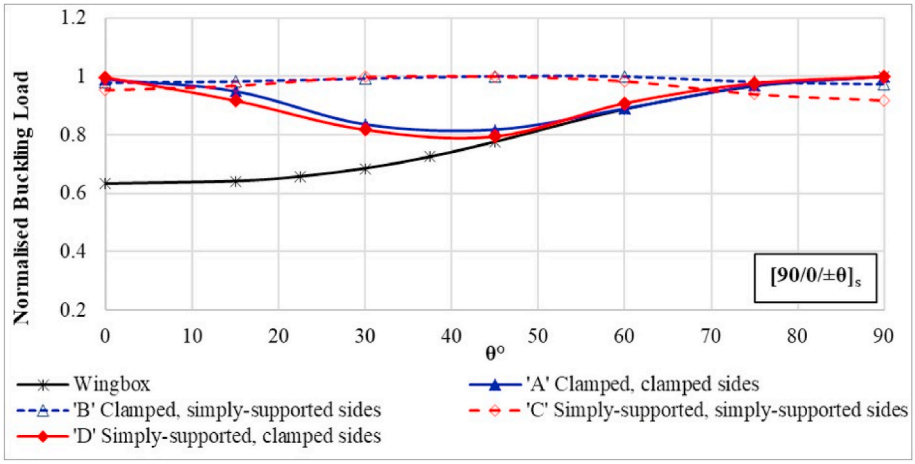

Fig. 6. FE parametric study: Non-dimensional buckling load as a function of fibre orientation (θ) for a wingbox structure under shear and moment loading, and for flat panels under pure compression. A lay-up of $[90/0/\pm\theta]_s$ is used for the skin in all cases.

90°. These correspond to lay-up sequences of $[90/0/0/0]_s$ and $[90/0/90/90]_s$ respectively. The trends for the pure compression tests of a simple panel under clamped and simply-supported boundary conditions show significant differences (Fig. 6). With all edges clamped (condition 'A'), the largest buckling load occurs at $\theta = 90°$, with the minimum occurring at $\theta = 45°$. Conversely, the maximum buckling load obtained in the simply-supported case (condition 'C') is achieved when $\theta = 45°$.

It is worth noting the influence of the edge boundary conditions for the pure compression tests (Fig. 6). When the edges are clamped, lateral Poisson's ratio expansion effects are resisted under loading, resulting in an induced bi-axial stress state developing. In this case, the primary loads are therefore aligned with the $\theta = 0°$ plies (direction of load introduction in the pure compression case) and with the 90° plies (aligned with the Poisson's ratio induced loads). The largest buckling load is achieved with $\theta = 0°$ and $\theta = 90°$, regardless of whether clamped or simply-supported boundary conditions are used at the load

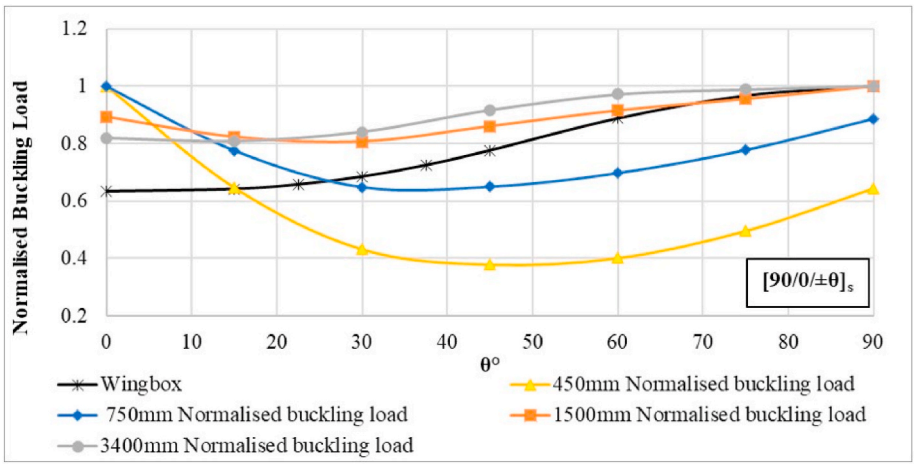

Fig. 7. FE parametric study: Normalised buckling load as a function of fibre orientation (θ) for a wingbox structure under shear and moment loading, and for bending-induced buckling test of the stiffened panel.

introduction sites. Likewise, the smallest buckling load is achieved when $\theta = 45°$.When the sides are simply-supported, the panel is permitted to expand or contract in the width-wise direction, resulting in no Poisson's ratio effect loads developing. As such, maximum buckling is achieved for $\theta = 45°$.

These differences show the deficiencies of pure-compression tests at capturing structural level type behaviour, such as the wingbox test. Careful thought is needed to choose boundary conditions which represent those of the actual structure being considered, otherwise misleading results may be obtained, leading to inappropriate conclusions. This consideration implies that such a test cannot be used to simulate the wingbox behaviour well, showing the need for an intermediate test.

The performance of the stiffened panel model compared to the wingbox is shown in Fig. 7. Interestingly, at low aspect ratios, the behaviour of the stiffened panel is similar to pure compression tests with clamped sides ($\theta = 45°$ results in a minimum buckling load). By increasing the length to 1500 mm (twice that of the wingbox section) behavioural changes occur with an S-shaped trend emerging with maximum buckling load at $\theta = 90°$. The loads are introduced at the panel mid-length, so each half of the stiffened panel behaves similarly to the wingbox in this case, showing that when the appropriate length is chosen, the intermediate test captures the appropriate behaviour, showing the test method is representative of the wingbox test; albeit that the absolute difference in buckling load is smaller than that for the wingbox case. This result shows the versatility of the proposed test method to represent different structural components at much less expense and time to set up the full-scale test.

4. Experimental test demonstration

4.1. Overview, design and manufacture

An experimental campaign was undertaken to validate our numerical models, gaining insight into the buckling mechanisms (through surface displacement and strain data) and to verify the simplicity of the test method. Two identical panels were manufactured and tested in order to assess repeatability of the method. The parameters of the tested panels (length, width, distance between stringers, and skin lay-up) were identified, based on previous results [21] and the available test equipment, such that the length of the panel was fixed at 750 mm. The remaining parameters are discussed in the following sections.

A parametric study (through FE models, as described in Section 3.1) was performed to determine the lay-up sequence used in experiments, as well as to gain further insight into the behaviour of the test method. As a consequence, a six-layer lay-up with stacking sequence of $[\pm\theta/90]_s$ was selected because the 90° layer was found to be better performing than 0°, and other ply angles are excluded to ensure balanced and symmetric laminates. The skin-stiffener bond strength was found to be insufficient when the number of layers was greater than six. This conclusion can be drawn by examining data shown in Fig. 8, where the buckling load is

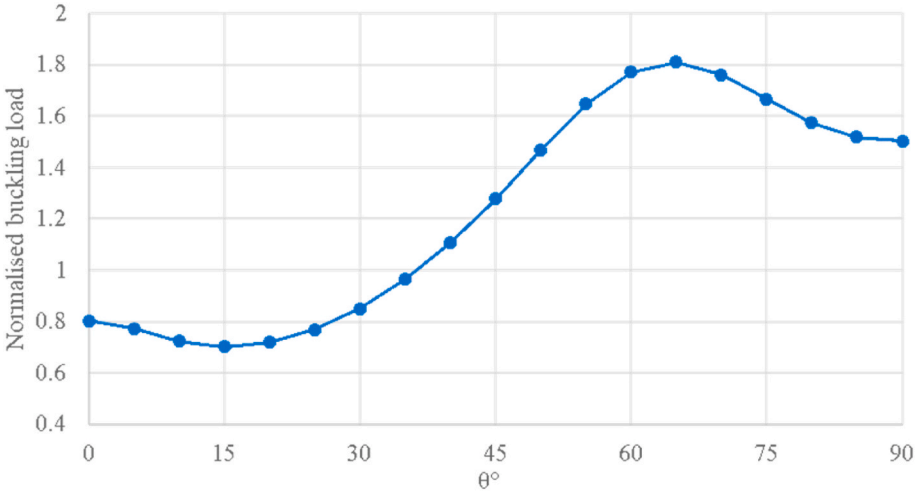

Fig. 8. FE predicted buckling load normalised with respect to a QI lay-up for a $[\pm\theta/90]_s$ layup.

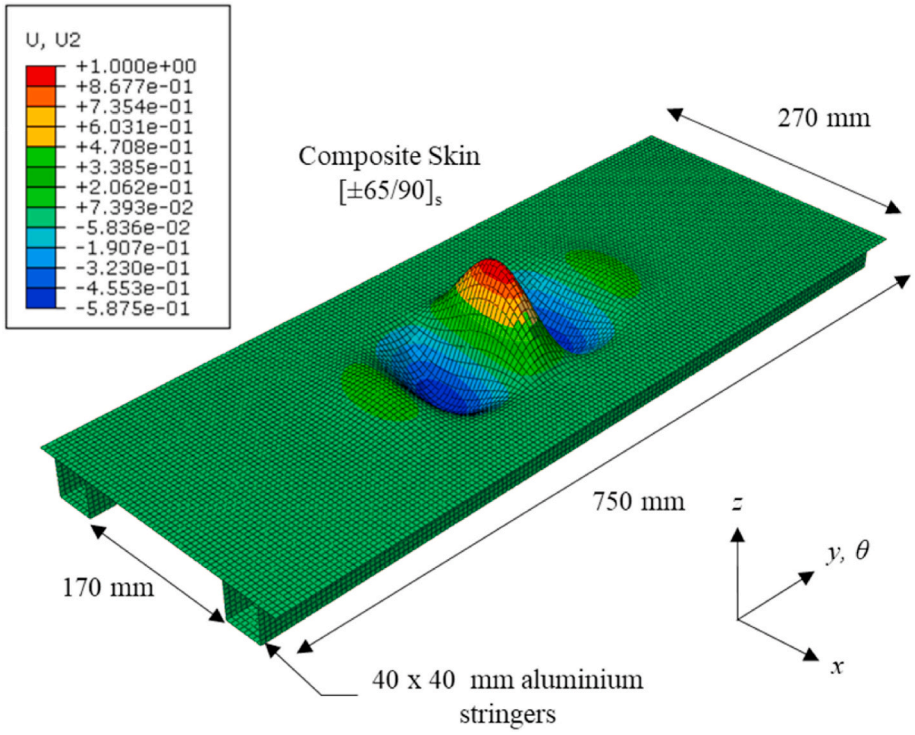

Fig. 9. Predicted first buckling mode from an FE linear buckling analysis (U2 refers to the total displacement vector).

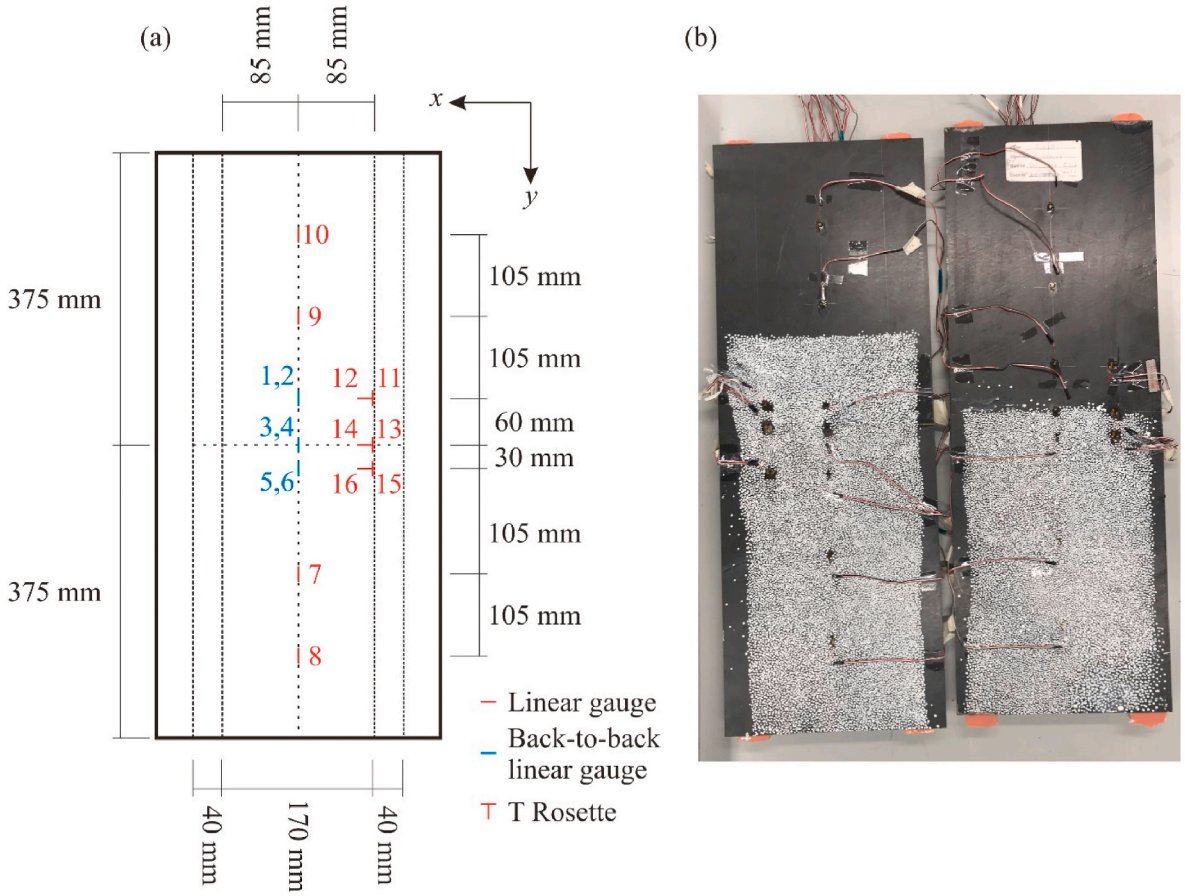

Fig. 10. (a) Strain gauge locations, orientation and identifier number on the stiffened panels; and (b) stiffened panels tested, showing strain gauges and Digital Image Correlation (DIC) speckling pattern.

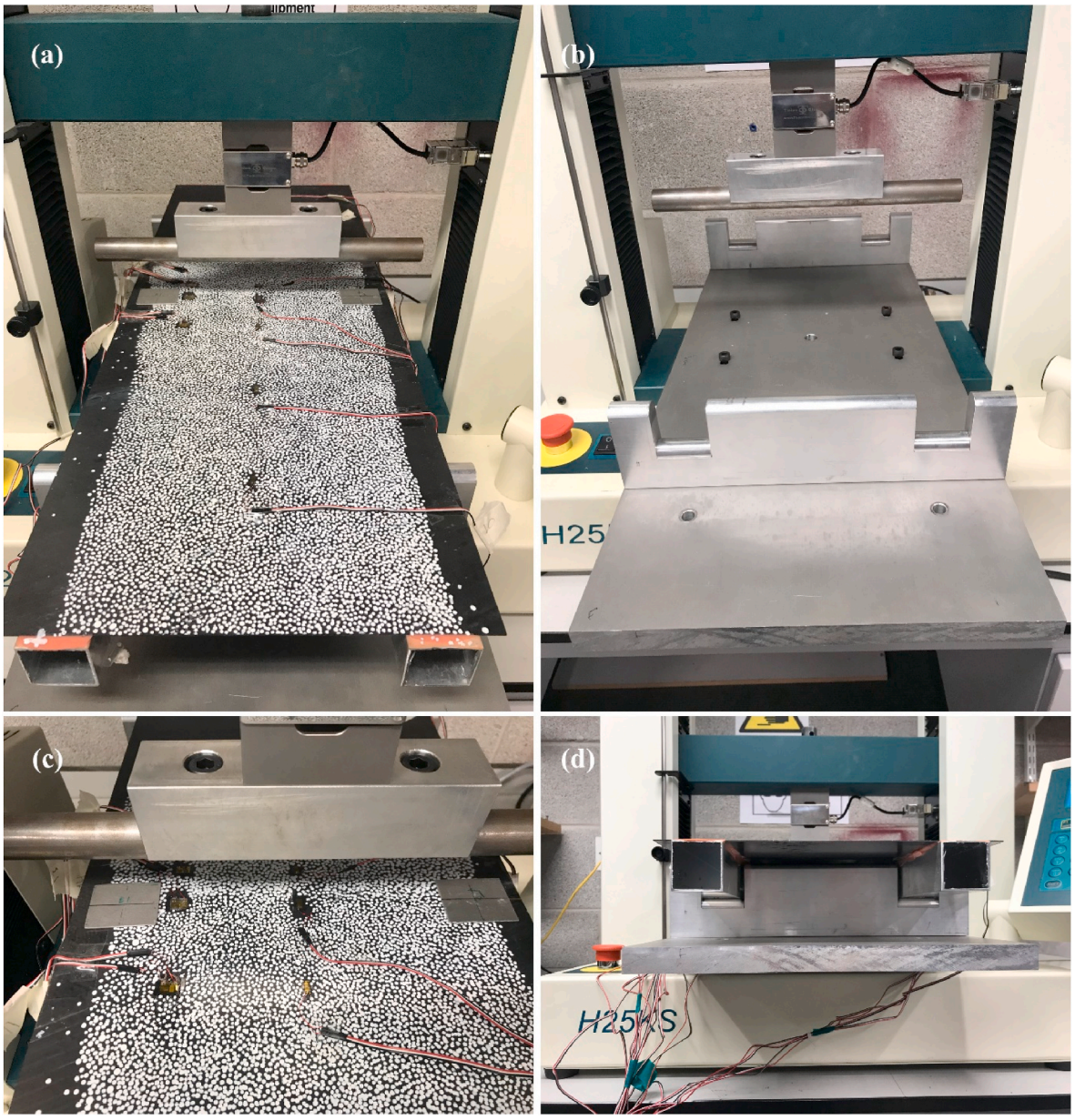

Fig. 11. (a) Stiffened panel loaded in the Tinius Olsen universal testing machine; (b) the supports and loading nose used; (c) The load introduction area with two aluminium spreader plates over the stiffeners; and (d) the simply-supported boundary condition supporting the stiffeners only.

normalised with respect to a quasi-isotropic (QI) lay-up, noting the buckling load of a QI panel is 1881 N. The maximum buckling load occurs when $\theta = 65°$, and is 3405 N, and so the final lay-up for the tested panel was chosen to be $[\pm 65/90]_s$.

4.1.1. Manufacturing

The geometry, lay-up and predicted buckling behaviour of the stiffened panel is shown in Fig. 9. The CFRP skin section was manufactured using Laser Assisted Tape Placement (LATP). This process uses an automated robotic arm to both lay down a tow of carbon fibre tape (6.35 mm width in this case) and consolidate the material in-situ using a laser heat source.

The inner (90°) layers of the skin section were manufactured first by winding tapes around a box-section tool. Two sections were cut from the wound piece, which then formed the mid-plies of the two panels. These sections were secured to a flat surface, and a −65° layer was laid down. The panel was then inverted and −65° and 65 layers were added. Finally, the panel was reverted to its original orientation to lay down the final 65° layer. This process was done because manufacturing the 90° layers first simplifies the process, while the inversion process was required to reduce thermal warping arising from unsymmetrical lay-ups occurring during the manufacturing process. Finally, the panels were post-processed in an autoclave at 340 °C and 7 bar of pressure for 2 h to remove possible residual warping effects.

3 M™ Scotch-Weld™ 9323-150 B/A epoxy adhesive was then used to bond the two aluminium stiffeners to the skin. Both aluminium and composite surfaces were prepared for bonding by abrading with emery paper and then cleaning with acetone. Spacers were used to position the stiffeners, and weights were used to provide pressure while the adhesive cured.

4.2. Test instrumentation and procedure

Experimental tests were undertaken to measure load, strains and surface displacements. These variables were chosen (a) to determine the buckling load; (b) to provide insight into the loads introduced into the

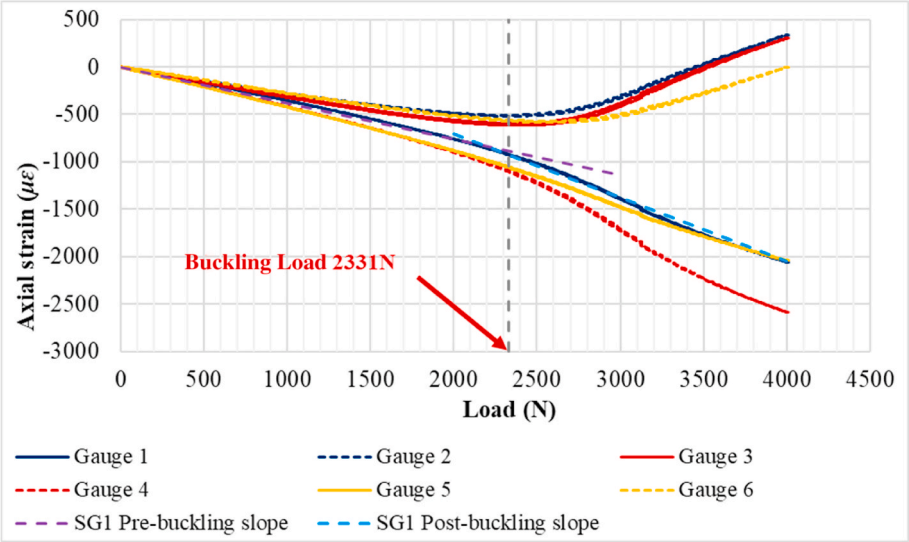

Fig. 12. Back-to-back strain data from panel 1.

panel and (c) to validate the FE simulations. Both panels were instrumented identically using 10 linear, 3 T-rosette strain gauges and Digital Image Correlation on one side. The positioning of the gauges is given in Fig. 10.

Gauges 1–6 were placed back-to-back on both top and bottom surface of the skin to capture the first and second buckling mode shapes predicted from FE models. Gauges 7–10 were placed to monitor the build-up of strain (and thus stress) along the length of the panel. Gauges 11–16 were placed to monitor the Poisson's effect adjacent to the stiffener.

Digital Image Correlation (DIC) was used as an optically based non-contact method to measure the three-dimensional surface displacements of the stiffened panel during loading. A LaVision Strainmaster system was used for both measurements and postprocessing. A calibration was performed in accordance with the manufacturer's procedures. The speckle pattern used for DIC, along with the complete test setup is shown in Fig. 11. It is worth highlighting that the panel is supported only at the stringers, and the bottom of the skin does not contact any of the supports.

A Tinius Olsen HK25S universal load tester was fitted with a 25 kN load cell. The test fixture (shown in Fig. 11(b)) was manufactured from 20 mm thick aluminium to assure sufficient rigidity. The bottom surfaces of the stiffeners were supported using rounded edges to provide the simply-supported boundary conditions. Likewise, load introduction was achieved using a 20 mm diameter steel bar; a loading rate of 2 mm/min was applied until a load of 4 kN was achieved. A centre line was marked on each panel to visually align the centre of the panel with the load introduction nose. This arrangement was used since any small misalignment, although not significantly affecting the buckling load, does alter strains as measured from the strain gauges. Square aluminium plates, measuring 40 × 40 × 1.5 mm were placed under the load introduction nose directly over the stiffeners. This arrangement ensures the load is applied in the region directly above the stringer, as done in the FE models (Fig. 4). The addition of the plates also reduces stress concentrations at load introduction points, while providing a gap between the loading nose and the skin material between the two stringers. This gap accommodated strain gauge 3, which was placed directly under the loading nose, and also ensures the centre part of the skin is unsupported and thus free to buckle. This addition of the plates was not incorporated in FE models because the spreader plates are not bonded to the skin, and as such, they are not expected to have a significant effect on the mechanics of the test. Finally, loading trials were conducted during the experimental set-up of both panels which indicated repeatable and consistent behaviour.

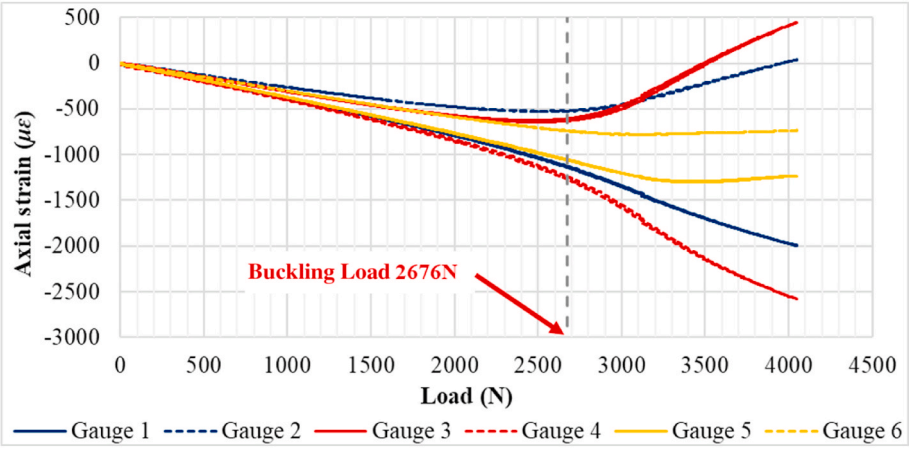

Fig. 13. Back-to-back strain data from panel 2.

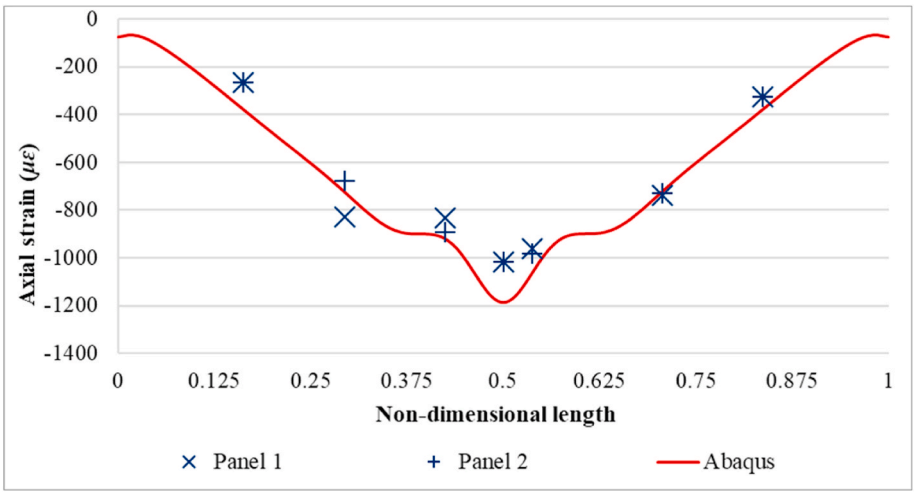

Fig. 14. Panel 1 and Panel 2, ϵ_{11} at 1.25 of buckling load. Note: ϵ_{11} shown are for the top surface only in both FE and experiments.

4.3. Test results

4.3.1. Surface strains

The first data examined concerns strains from the back-to-back gauges at the centre of the panel (gauges 1–6) for panel 1 and 2 (Fig. 12 and Fig. 13, respectively). These plots show the development of ϵ_{11} during loading. During the initial stages of loading (0–2 kN) the gauges show some divergence. This behaviour is expected as the panel is under bending, resulting in a strain gradient through the skin. Additionally, any initial imperfection in the skin (e.g. initial curvature) also contributes to this divergence. As buckling involves local bending of the skin section at the strain gauge location, the onset of buckling can be observed from the point at which back-to-back gauges show a change in the rate of divergence between them, referred to as the 'inflection point' method in Ref. [22]. This method is also used in, for instance Refs. [23, 24], and basically relies on the fact that when a plate buckles, the back-to-back strain gauges suddenly diverge. However, as some gauges show a gradual transition into buckling, the inflection point [22] was used to provide a buckling load. The intersection point of the pre- and post-buckling linear slope was extracted for each strain gauge, and the average value used to provide a buckling force value. The extracted slopes for Strain Gauge 1 (SG1) are shown as an example in Fig. 12. Using this method, buckling loads of 2331 N and 2676 N were extracted for Panels 1 and 2, respectively, with an average value of 2503 N.

Following buckling, (i.e., post 2331 N for panel 1, Fig. 12), gauge 3 shows a decrease in compressive strain, eventually transitioning into tension at approximately 3500 N. Gauge 4, which is the corresponding gauge on the bottom skin, shows an increase in the rate in compressive strain. This result shows the formation of a buckling half wave, displacing in the positive z direction (refer to Fig. 9 for the coordinate system used). Monitoring the strains at back-to-back gauges 1 and 2 reveals another buckling half wave, orientated in the negative z direction. These behaviours are repeated for panel 2 (Fig. 13). The back-to-back gauges 5 and 6 show a minor difference in behaviours between the two panels. In panel 1, the gauges show a clear divergence after buckling, indicating that the gauges are placed in a position of localised bending where a strain gradient exists across the skin thickness. Therefore, another buckling half-wave exists at this location. For panel 2, however, the divergence is less obvious. Indeed, gauge 5 shows a decrease in compressive strain, while gauge 6 shows the strain remains roughly constant. There is relatively no divergence in strains observed between these two gauges following buckling. This data indicates that there is minimal localised bending at this point, and thus the buckling half wave that occurred in panel 1 at this location may be displaced slightly away from these gauges in panel 2. Full field displacement results from DIC are used to verify this observation in Section 4.3.2.

Next, the development of strain along the length of the panel is compared against that predicted by non-linear FE analysis at 1.25 times the buckling load. This non-linear analysis was done using the same model as used for the parametric study, with a small geometrical imperfection in the shape of the first buckling mode introduced. The longitudinal strains, ϵ_{11} were extracted along gauges 1, 3, 5, 7–10 for panel 1 (at 2823 N) and panel 2 (at 2963 N). These were plotted as a function of non-dimensionalised panel length, as shown in Fig. 14.

Fig. 14 shows that the data points from experiments follow the strain profile predicted by FE analysis. This close correlation indicates that the

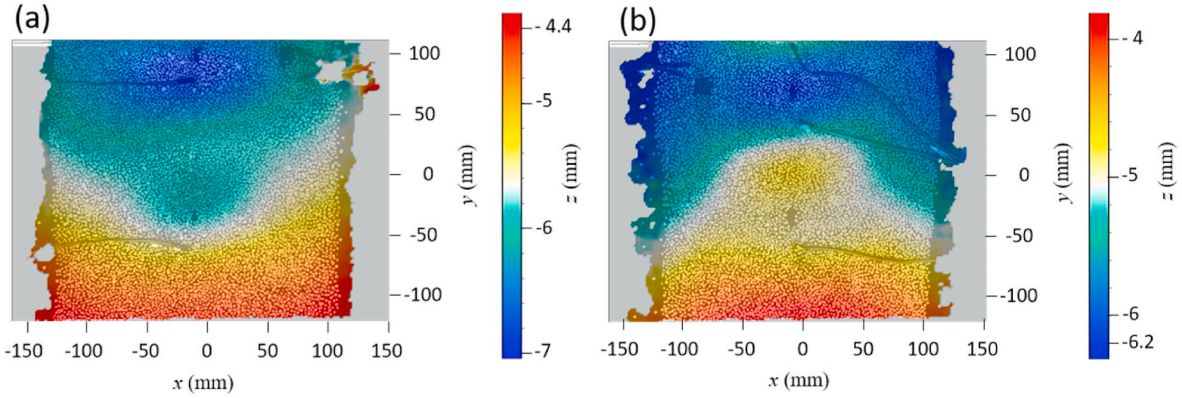

Fig. 15. DIC measured out-of-plane displacements for (a) panel 1 (4010 N); and (b) panel 2 (4050 N).

experimental buckling mode was captured well by FE analysis as further verified by DIC results in Section 4.3.2. The predicted buckling value from FE modelling was 3405 N, while the average value experimentally observed was 2503 N. This difference is to be expected due to the presence of imperfections in the manufactured laminate (e.g. fibre misalignment; gaps due to variation in the tape width). The ϵ_{11} measured shows good correlation for the bending behaviour of the laminate, as the data points at the outer sections closely match those predicted by FE analysis. In the centre section of the laminate, where buckling half-waves are present, the measured strains are lower than those predicted ($-1000\ \mu\epsilon$ compared to $-1200\ \mu\epsilon$). This difference indicates that the buckling wave is not as pronounced as predicted, a consequence of the reduced buckling load in the experiments.

4.3.2. Full-field displacements

The full-field displacements in the post-buckling regime were measured to further verify the buckling mode obtained. These were measured using DIC, and are shown at the peak experimental load (i.e., 4 kN) in Fig. 15. DIC was used to monitor the displacements over half of the panel length, with negative displacements in the z-direction being a result of bending the panel so that the skin is in compression (as per Fig. 11). Note that the view of the centre of the panel is blocked from the DIC cameras by the loading nose and so no displacement data is available in this area.

The global bending deformation is shown by the gradual increase in out-of-plane displacements at the load introduction area of the panel. The buckling patterns are also clearly visible in both images, which match the first buckling mode predicted (Fig. 9). The half-wave with increased negative displacement readings indicates a negative half wave (buckle towards the stringers), while an area of decreased negative displacements indicates a positive half-wave.

Panel 2 shows a more pronounced second buckle than Panel 1 as observed by strain gauge 5 (see section 4.3.1). Due to the loading nose blocking the view of the DIC camera, displacements at the centre of the panel are not available.

It is worth noting that the measured displacements did not indicate debonding of either of the stringers, as the displacements remain symmetrical about the panel's mid-width. If debonding had occurred, the displacements around the de-bonded section would have shown a local deviation. Likewise, the strain readings given in Figs. 12 and 13 show a continuous build up in strain during loading, with no step changes in readings which would have indicated debonding had occurred.

5. Discussion

5.1. New test method

The new test method is simple in ethos, quick to execute, with boundary conditions which are easy to implement in modelling and testing. Positioning the panel is extremely straightforward and requires that the stiffeners are only placed in the Computer Numerically Controlled (CNC) cut grooves in the test frame for alignment, as these are accurately controlled during the manufacturing of the test frame. Therefore, the boundary conditions can largely be eliminated as a source for any deviation from the expected behaviour during the test, greatly facilitating the analysis of results.

The test did show a lower buckling load than that anticipated from models, however (≈2503 N versus 3405 N). This large reduction is attributed to a combined effect of a number of factors. Firstly, although the carbon fibre tapes were placed using an automated process, some manual repositioning of the laminate was required during manufacture. This process can lead to misalignments in the fibre trajectories, which were chosen to give the highest buckling load as per a performed parametric study. Any deviation from these trajectories will therefore reduce buckling loads. In addition, the manufacturing process uses high temperatures for material processing, resulting in the formation of thermal residual stresses, resulting in the panels warping to a small degree, which remained in the area between the stiffeners after they were bonded on. Even though curing of the stiffeners in the autoclave process flattened the panels to a large degree, some thermal stress is expected to have remained in the panels, having a detrimental effect on the buckling load. Consequently, the mismatch between predicted and measured buckling loads can be attributed to the defects induced by panel manufacturing process. With different materials or construction types (e.g. a homogeneous metallic skin section), a good match is expected.

Some misalignment in the longitudinal placement of the panel was observed by reading strain gauge data. This problem occurred despite attempts to place the centre of the panel directly under the loading nose. When strain gauges are used, their location must be carefully recorded with respect to the actual load introduction point, and so it is recommended that additional measures are taken to ensure the panel is centred. It is worth noting that the lengthwise centring achieved here does not change the measured buckling load, yet changes the location of the strain gauges relative to the loading edge, which influence the measured strain values.

The comparison with large scale tests (wingbox) shows the importance of progressing to using tests that capture complex behaviours of actual structures. Traditional axial compression tests show widely different behaviours depending on the nature of the boundary conditions. These tests must be carefully chosen to simulate the loading of the actual structure of interest, otherwise inappropriate results may be obtained. Our new test captures the physics of a stiffened panel in bending to a high degree, accounting for through-thickness stress variation and Poisson's ratio effects, at a fraction of the time and cost of performing a large-scale test.

In addition, the test is also easily adaptable to represent different structural load applications. Firstly, the length between supports (boundary edges) is adjustable, to provide different ratios of bending moment to shear load, as required. Should only a constant bending moment be required over the length of the test section, a 4-point bend test can be used instead. In addition, changing the flexural stiffness and/or geometry of the stiffeners changes the through-thickness stress gradient in the skin. The test configuration can also be used to control the test fixture design, to ensure loads are kept within desired levels for strength of test apparatus considerations. For example, increasing the length between supports results in a desired bending moment being achieved with a smaller shear force. Other configurations may also be considered, such as a combined compression and torsion case (by adjusting the height of the supports) or use of a curved panel, which is not possible to test using regular axial tests.

Finally, the numerical model of the skin section also replicated the behaviour of the full-scale numerical model of the wing, yet at less than 5% of the time and cost to run such a complex model. Therefore, the proposed test configuration could be used in a modelling case to test more complex structural behaviours. Optimisation studies could also benefit from this observation.

5.2. Physical understanding of the new test method

To understand the parametric study performed in Section 4.1.1, and to gain insight into the physics behind the test method, an analogy with bi-axial loading is drawn. As already mentioned for the clamped boundary conditions in a pure compression test, a bi-axial compression state exists due to the lateral sides being prevented from expanding (Poisson's effect). Since in the new test method the stiffeners resist in-plane deformation arising from Poisson's effects, a bi-axial loading state also exists in the new test set-up. Hence, even though the buckling load is dictated by the out-of-plane stiffness matrix $\boldsymbol{D}$, the additional loading arises due to the pre-buckling in-plane stiffness and the load introduced by the plate not being allowed to expand.

Assuming that the strain in y-direction ε_y and the shear strain κ_{xy} are

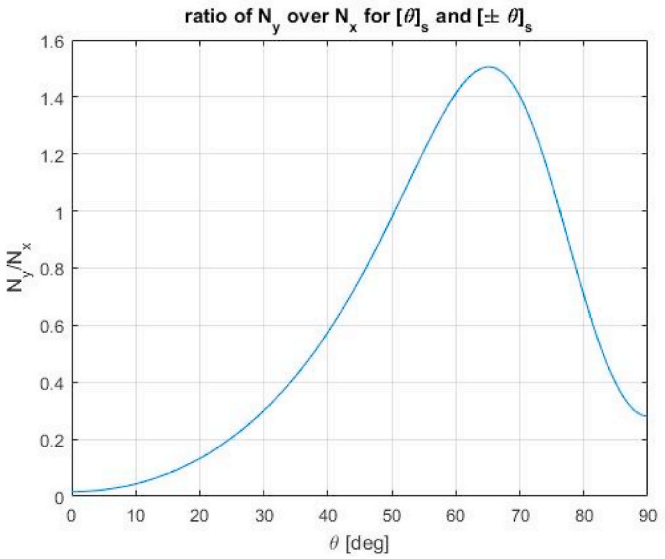

Fig. 16. Ratio of *Ny* over *Nx* as a function of θ for $[\pm\theta]_s$ and $[\theta]$.

zero (i.e., being prevented by the stiffeners), and the laminate is symmetric, force and strain are related as:

$$\begin{bmatrix} N_x \\ N_y \\ N_{xy} \end{bmatrix} = \begin{bmatrix} A_{11} & A_{12} & A_{16} \\ A_{21} & A_{22} & A_{26} \\ A_{61} & A_{26} & A_{66} \end{bmatrix} . \begin{bmatrix} \varepsilon_x \\ 0 \\ 0 \end{bmatrix} \tag{1}$$

where $\boldsymbol{N}$ denotes the normal stress resultant and $\boldsymbol{A}$ is the in-plane stiffness matrix. From Eqn. (1) then

$$\frac{N_y}{N_x} = \frac{A_{12}}{A_{11}}$$
$$\frac{N_{xy}}{N_x} = \frac{A_{16}}{A_{11}} \tag{2}$$

Therefore, no shear force exists if the laminate is symmetric and balanced. To compare to previous results from Weaver [21] concerning induced secondary stress states in composite panels, a stacking sequence of $[\pm\theta]_s$ is used. This stacking sequence is symmetric, hence the above formulas hold.

For the laminates the ratio of N_y to N_x as a function of θ is shown in Fig. 16. For θ between 50° and 75° it is perhaps surprising that the force in the *y*-direction is larger than the force in the *x*-direction. The maximum force appears at an angle of around 65° which is the angle that was found to be the best angle (in combination with two 90° plies in the middle) in the parametric study. The magnitude of the force N_y is larger than that used by Weaver, but still the general trend matches relatively well, as can be observed by comparing Figs. 17 and 18. The initial drop shown in Fig. 18 can be explained by the increase in N_y. The largest buckling load obtained occurs at a larger angle than in Ref. [21], which can also be attributed to the larger value of N_y as the largest buckling load occurs for larger angles when the ratio of N_y to N_x increases. Another notable fact is the higher tensile force due to the 90° ply than the 0° ply. This effect is the reason the 90° ply leads to a higher buckling load than the 0° ply, and hence justifies the choice of having a 90° ply rather than a 0° ply at the symmetry plane.

A similar result was also found by Sebaey et al. [25] who optimised a plate under bi-axial compression for highest failure load. The failure load was defined as either buckling occurring or a failure criterion being violated. For a ratio of N_y to N_x of 0.125, the optimal laminate was found to consist of ±45° and ±50° plies. When the ratio is increased to 0.25, the optimal laminate consists of ±50°, ±55° and ±60° plies. For a ratio of 0.5, the optimal laminate consists of ±60° and ±65° plies. Hence, the general trend is that the larger the ratio of N_y to N_x, the greater the optimal fibre angles become. Hence, combining the information on the ratio of the forces and the optimum angle obtained in this work, results between the two studies are similar.

6. Conclusions

A simple method for testing the compression buckling response of stiffened panels has been proposed and a proof-of-concept has been given using a combination of experiments and FE modelling. A FE based modelling and parametric study comparing the proposed test against traditional pure compression tests and full-scale wingbox section tests showed that the proposed test captures the behaviour of large-scale tests (in this example a wingbox) in a representative manner, while conversely conventional, standard compression tests can produce varying and misleading results, as was shown by the different trends in buckling load when varying the lay-up. These additional behaviours, captured using the proposed method, include an in-plane variation in bending moment, as well as a bi-axial stress state due to Poisson's effects which cannot be captured using conventional standard buckling tests

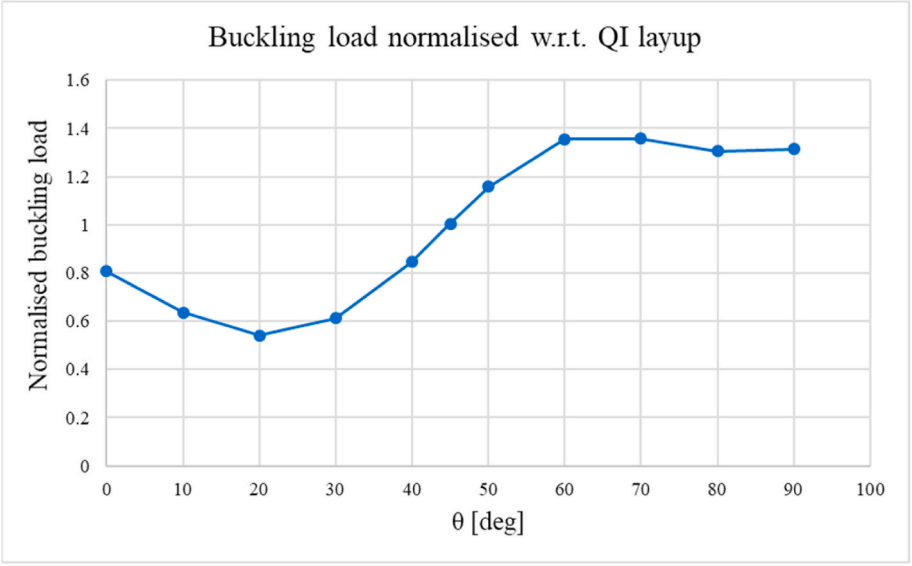

Fig. 17. Normalised buckling load with respect to the QI layup of $[\pm\theta]_s$ layup.

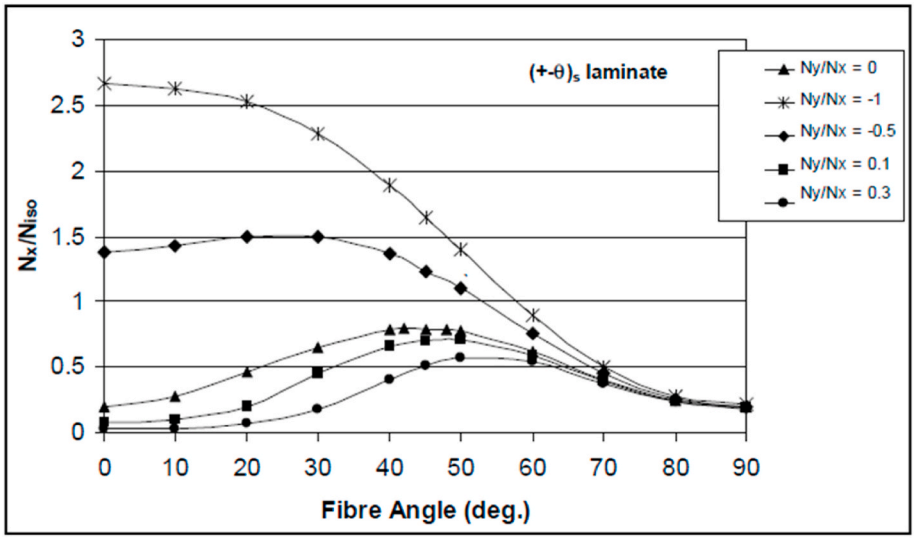

Fig. 18. Normalised buckling load for a bi-axially loaded plate from Weaver [21].

due to their non-representative boundary conditions. Digital Image Correlation and strain gauge results from experiments were used to verify the proposed method. Simple adjustments to the test frame (e.g. length, three- or four-point bending) can be made to tailor the bending moment, shear force and through-thickness stress distribution of an actual structure.

The results show that the proposed testing method, which exploits bending instead of compression to induce buckling, is simpler to perform, more cost-effective, more robust and more representative of stiffened panels subjected to buckling in real structures than the small coupon test that introduce pure compression into the coupons.

Authorship statement

Category 1.

Conception and design of study/methodology: R. Telford, D.M.J Peeters, M. Rouhi, P. M. Weaver;

Acquisition and processing of data: R. Telford, M. Rouhi;

Analysis and/or interpretation of data: R. Telford, D.M.J Peeters, M. Rouhi;

Category 2.

Drafting the manuscript: R. Telford, D.M.J Peeters, M. Rouhi;

Revising the manuscript critically for important intellectual content P.M. Weaver.

Category 3.

Approval of the version of the manuscript to be published (the names of all authors must be listed):

R. Telford, D.M.J Peeters, M. Rouhi, P.M. Weaver.

Declaration of competing interest

The authors declare that they have no known competing financial interests or personal relationships that could have appeared to influence the work reported in this paper.

Acknowledgment

The authors would like to thank Science Foundation Ireland for funding the Spatially and Temporally Variable Composite Structures grant no. (15/RP/2773) under its Research Professor program. The authors would also like to thank Irish Composites Centre (ICOMP) for its help with the laser-assisted automated tape placement.

References

[1] Parida BK, Prakash RV, Ghosal A, Mangalgiri PD, Vijayaraju K. Compression buckling behavior of laminated composite panels. In: Composite materials: testing and design, thirteenth volume. ASTM International; 1997.

[2] Zucco G, Oliveri V, Peeters D, Telford R, Clancy GJ, McHale C, et al. Static Test of a thermoplastic composite Wingbox under Shear and bending moment. In: 2018 AIAA/ASCE/AHS/ASC structures, structural dynamics, and materials conference. AIAA; 2018.

[3] Balbin C, Bisagni M, Schultz, Hilburger M. Scaling Methodology for buckling of sandwich composite cylindrical structures. In: AIAA/ASCE/AHS/ASC structures, structural dynamics, and materials conference. AIAA SciTech Forum, (AIAA 2018-1693); 2018.

[4] Oliveri V, Zucco G, Peeters D, Clancy G, Telford R, Rouhi M, McHale C, O'Higgins RM, Young TM, Weaver PM. Design, manufacture and test of an in-situ consolidated thermoplastic variable-stiffness wingbox. AIAA J 2019;57(4):1671–83.

[5] McCrory JP, Al-Jumaili SK, Crivelli D, Pearson MR, Eaton MJ, Featherston CA, Guagliano M, Holford KM, Pullin R. Damage classification in carbon fibre composites using acoustic emission: a comparison of three techniques. Compos B Eng 2015;68:424–30.

[6] Schuman L, Back G. Strength of rectangular flat plates under edge compression. 1931.

[7] Hofmayer H, Jaspart JP. On the modelling of compressed long plates related to sheet-section behaviour. In: Fifth international conference on thin-walled structures; 2008. Brisbane, Australia.

[8] Starnes J, Knight N, Rouse M. Postbuckling behavior of selected flat stiffened graphite-epoxy panels loaded in compression. AIAA J 1985;23(8):1236–46.

[9] Richardson MOW, Zhang ZY, Wishearth M, Tyrer JR, Petzing J. ESPI Non-destructive testing of GRP composite materials containing impact damage. Comp Part A 1998;29A:721–9.

[10] Perret A, Mistou S, Fazzini M, Brault R. Global behaviour of a composite stiffened panel in buckling. Part 2: Exp Investig Compos Struct 2012;94(2):376–85.

[11] Seide P, Stein M. Compressive buckling of simply supported plates with longitudinal stiffeners. 1949.

[12] Falzon BG, Stevens KA, Davies GO. Postbuckling behaviour of a blade-stiffened composite panel loaded in uniaxial compression. Compos Appl Sci Manuf 2000;31(5):459–68.

[13] Bisagni C, Vescovini R, Dávila CG. Single-stringer compression Specimen for the Assessment of damage Tolerance of postbuckled structures. J Aircraft 2011;48(2):495–502.

[14] Rouhi M, Ghayoor H, Fortin-Simpson J, Zacchia TT, Hoa SV, Hojjati M. Design, manufacturing, and Testing of a variable stiffness composite cylinder. Compos Struct 2018;184:146–52.

[15] Przekop A, Schultz MR, Hilburger MW. Design of buckling-critical large-scale sandwich composite cylinder test articles. In: 2018 AIAA/ASCE/AHS/ASC structures, structural dynamics, and materials conference; 2018.

[16] Abramovich H, Weller T. Buckling and postbuckling behavior of laminated composite stringer stiffened curved panels under axial compression: Experiments and design guidelines. J Mech Mater Struct 2009;4(7):1187–207.

[17] Zimmermann R, Klein H, Kling A. Buckling and postbuckling of stringer stiffened fibre composite curved panels – Tests and computations. Compos Struct 2006;73(2):150–61.

[18] Bisagni C, Dávila CG. Experimental investigation of the postbuckling response and collapse of a single-stringer specimen. Compos Struct 2014;108:493–503.

[19] Bisagni C, Vescovini R, Dávila CG. Single-stringer compression specimen for the assessment of damage tolerance of postbuckled structures. J Aircraft 2011;48(2):495–502.
[20] Inc ASM. Aluminum 6063-T6 technical data" ASM.matweb.com. http://asm.matweb.com/search/SpecificMaterial.asp?bassnum=MA6063T6. [Accessed 29 November 2018].
[21] Weaver P. Design formulae for buckling of biaxially loaded laminated rectangular plates with flexural/twist anisotropy. In: 46th AIAA/ASME/ASCE/AHS/ASC structures, structural dynamics and materials conference; 2005.
[22] Paszkiewicz Maria, Kubiak Tomasz. Selected problems concerning determination of the buckling load of channel section beams and columns. Thin-Walled Struct 2015;93:112–21. https://doi.org/10.1016/j.tws.2015.03.009. ISSN 0263-8231.
[23] Abramovich H, Bisagni C. Behavior of curved laminated composite panels and shells under axial compression. Prog Aerospace Sci 2015;78:74–106. https://doi.org/10.1016/j.paerosci.2015.05.008. ISSN 0376-0421.
[24] Coan JM. Large-deflection theory for plates with small initial curvature loaded in edge compression. 1951. p. 143–51.
[25] Sebaey TA, Lopes CS, Blanco N, Costa J. Ant Colony Optimization for dispersed laminated composite panels under biaxial loading. Compos Struct 2011;94(1):31–6.